Crystal structure and mechanistic determinants of SARS coronavirus nonstructural protein 15 define an endoribonuclease family

Stefano Ricagno*, Marie-Pierre Egloff*, Rachel Ulferts†, Bruno Coutard*, Didier Nurizzo‡, Valérie Campanacci§, Christian Cambillau§, John Ziebuhr†, and Bruno Canard*¶

Cases *925 and §932, Ecole d'Ingénieurs de Luminy, Architecture et Fonction des Macromolécules Biologiques, Unité Mixte de Recherche 6098, Centre National de la Recherche Scientifique and Universités d'Aix-Marseille I et II, 163 Avenue de Luminy, 13288 Marseille Cedex 9, France; †Centre for Cancer Research and Cell Biology, School of Biomedical Sciences, Queen's University Belfast, 97 Lisburn Road, Belfast BT9 7BL, United Kingdom; and ‡European Synchrotron Radiation Facility, ID23, B.P. 220, F-38043 Grenoble Cedex, France

Edited by Charles M. Rice, The Rockefeller University, New York, NY, and approved June 23, 2006 (received for review March 1, 2006)

The ≈30-kb coronavirus (+)RNA genome is replicated and transcribed by a membrane-bound replicase complex made up of 16 viral nonstructural proteins (nsp) with multiple enzymatic activities. The complex includes an RNA endonuclease, NendoU, that is conserved among nidoviruses but no other RNA virus, making it a genetic marker of this virus order. NendoU (nsp15) is a Mn^{2+}-dependent, uridylate-specific enzyme, which leaves 2′–3′-cyclic phosphates 5′ to the cleaved bond. Neither biochemical nor sequence homology criteria allow a classification of nsp15 into existing endonuclease families. Here, we report the crystal structure of the severe acute respiratory syndrome coronavirus nsp15 at 2.6-Å resolution. Nsp15 exhibits a unique fold and assembles into a toric hexamer with six potentially active, peripheric catalytic sites. The structure and the spatial arrangement of the catalytic residues into an RNase A-like active site define a separate endonuclease family, endoU, and represent another spectacular example of convergent evolution toward an enzymatic function that is critically involved in the coronavirus replication cycle.

endonuclease | severe acute respiratory syndrome | nidovirus | replication

Coronaviruses possess the largest and most complex genome among RNA viruses [≈30 kb of single-stranded (+)RNA] (1). The family *Coronaviridae* (genera *Coronavirus* and *Torovirus*) belongs to the order *Nidovirales*, which also includes the *Arteriviridae* and *Roniviridae*. Translation of the coronavirus genome results in two replicase polyproteins (of ≈4,500 and ≈7,500 aa) that are encoded by ORFs 1a and 1b and are known as polyproteins pp1a and pp1ab, respectively (2). Expression of the pp1ab C terminus depends on a translation frameshift occurring just upstream of the ORF1a stop codon (3). Because of this translational regulation of gene expression, the five C-terminal proteolytic products, nonstructural protein (nsp)12 to nsp16, are produced at significantly lower amounts than are the ORF1a-encoded replicase subunits. Proteolytic processing of coronavirus pp1a and pp1ab by ORF1a-encoded proteases yields 15–16 nsp, which mediate the replication of the viral RNA genome and the synthesis of multiple subgenome-length mRNAs (4) that encode the structural and accessory proteins (2).

Recently, coronaviruses received both general attention and renewed interest after a worldwide outbreak of the severe acute respiratory syndrome (SARS) in 2003. The etiological agent of SARS was identified as a group II coronavirus, which was named SARS-CoV (5–7). The genome contains ≈29.7 kb and codes for 16 nsps, 5 structural proteins, and 7 accessory proteins (2). In the last two years, several of the SARS-CoV replicase subunits including a number of enzymatic activities have been characterized (reviewed in refs. 1 and 2). Furthermore, crystal structures of five nsps (or subdomains thereof) have been reported: the ADP-ribose-1″-phosphatase *macro* domain of nsp3, the main protease nsp5, the RNA-binding protein nsp9, and the complex of nsp7–nsp8, a proposed processivity factor for the RNA-dependent RNA polymerase nsp12 (8–12). nsp13 is a superfamily 1 helicase (7, 13), whereas nsp14, nsp15, and nsp16 have been predicted or confirmed to harbor 3′–5′ exonuclease, endonuclease, and 2′-*O*-ribose methyltransferase activities, respectively (7, 13–15). Among these, the nidovirus uridylate-specific endoribonuclease (NendoU) residing in nsp15 is considered a major genetic marker of nidoviruses because of its nidovirus-wide conservation but complete absence in other RNA viruses (16). The biochemical properties of nsp15 have been characterized to some extent, and the protein has been shown to be critical for coronavirus RNA synthesis (15–17). NendoU is distantly related with the *Xenopus laevis* endoribonuclease, XendoU, that is involved in the processing of intron-encoded box C/D U16 small, nucleolar RNA (18).

Catalytic features, such as metal-ion dependence, are often used to classify RNases into two main groups. The first group employs a two-metal-ion mechanism, with one ion activating the substrate and the second one stabilizing the transition state (19). In the second group, two side chains, typically those of His residues, act as a general base and general acid in a coordinated fashion to promote cleavage (20, 21). However, neither nsp15 nor XendoU can be easily assigned to one of these enzyme classes: in common with enzymes from the first class, NendoU and its homologs require metal ions for activity. However, unlike these enzymes, NendoU and XendoU generate 2′–3′ cyclic phosphates upon cleavage, which is a typical feature of RNases belonging to the second class (18). In previous studies, potential catalytic amino acid residues of NendoU have been identified by site-directed mutagenesis (16, 17), and the molecule has been reported to form monomers, trimers, and hexamers in solution (17). Here, we report the crystal structure of the SARS-CoV NendoU (nsp15) at 2.6-Å resolution. The folds of each of the three nsp15 subdomains and their spatial arrangement were found to be unprecedented. We also show that nsp15 assembles into hexamers presenting six independent catalytic sites at their periphery. The combined data define a novel family, endoU, of RNA endonucleases.

Results

The Monomer Structure. The nsp15 crystals we obtained contained one monomer per asymmetric unit. The experimental electron density, obtained from single-wavelength anomalous dispersion phasing to 2.9 Å on a selenomethionine-substituted crystal, was of sufficient quality to trace the whole chain, including residues 5 and

Conflict of interest statement: No conflicts declared.

This paper was submitted directly (Track II) to the PNAS office.

Abbreviations: SARS, severe acute respiratory syndrome; nsp, nonstructural protein

Data deposition: The atomic coordinates and structure factors have been deposited in the Protein Data Bank, www.pdb.org (PDB ID code 2H85).

¶To whom correspondence should be addressed. E-mail: bruno.canard@afmb.univ-mrs.fr.

© 2006 by The National Academy of Sciences of the USA

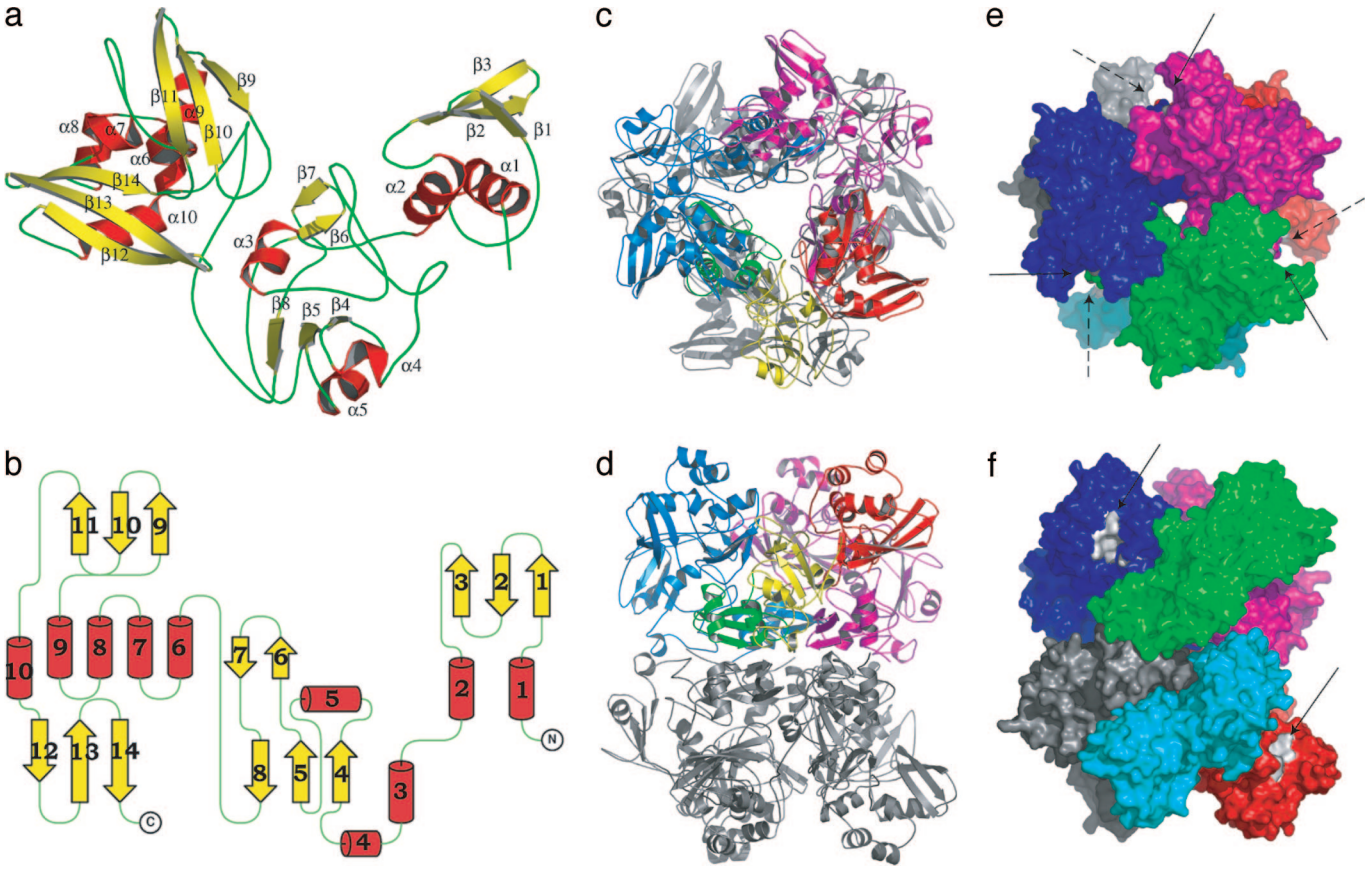

Fig. 1. Structure of nsp15, the endoribonuclease from SARS-CoV. (*a* and *b*) Cartoon representation (*a*) and topology diagram (*b*) of nsp15 monomer. The structure consists of three domains: N-terminal domain (α1–α2), central domain (α3–β8), and C-terminal domain (α6–β14). Secondary structures are colored as follows: red, α-helices; yellow, β-sheets; and green, loops. (*c*) A view of the nsp15 hexamer. In the trimer shown in the foreground, the subdomains of one of the monomers are colored as follows: green, N-terminal domain; yellow, central domain; and red, C-terminal domain. The other two molecules are shown in blue and magenta. The molecules belonging to the trimer in the background are shown in gray. (*d*) 90° rotation of the nsp15 hexamer as shown in *c*. (*e*) Surface representation of the nsp15 hexamer. Solid arrows indicate the active sites of the trimer in the foreground; dashed arrows show the active sites of the trimer in the background. (*f*) The hexamer shown in *e* is rotated by 90°. In this orientation, two active sites are visible, and they are highlighted by solid arrows and colored in white.

6, of the N-terminal affinity tag. The final model, refined at 2.6-Å resolution, is of high quality as judged by the electron density map (Fig. 4, which is published as supporting information on the PNAS web site) and by PROCHECK criteria (Table 1, which is published as supporting information on the PNAS web site). The protein selected for large-scale production and crystallization contained three mutations: the last His of the N-terminal His_6-tag was replaced with Gln, and two other residues, Val-291 and Asp-300, were replaced with Gly. The protein was confirmed to possess uridylate-specific endoribonuclease activity (Fig. 5, which is published as supporting information on the PNAS web site) and the temperature factors observed in the Gly-substituted regions were within average, indicating that the two replacements did not affect the nsp15 local structure.

The monomer consists of three domains of increasing size (Fig. 1*a*), a small N-terminal domain (residues −1 to 62), a central domain (residues 63–191) and a large C-terminal domain (residues 192–345). The connectivity and topology of the molecule are given in Fig. 1*b*. The N-terminal domain (α1–α2) is formed by a three-stranded antiparallel β-sheet with two helices packed against one of its sides. As many as 88 (of 128) residues of the central domain (α3–β8) are part of coiled regions. However, only a short stretch of amino acids, between positions 110 and 115, have temperature factors higher than average, probably because of the extensive solvent exposure of this particular segment. Helix α3 is connected by a 39-aa-long coil to an α/β region, consisting in two helices and five β-strands. A central three-stranded β-sheet (β4, β5, and β8) is covered on one side by two helices (α4 and α5), and two short antiparallel β-strands (β6 and β7) are inserted between strand β5 and β8. The C-terminal domain (α6–β14) contains an α-helical core (α6–α9) flanked on both sides by two antiparallel three-stranded β-sheets (β9–β11 and β12–β14). These two β-sheets form a groove that exhibits a positive electrostatic potential (see below).

A search on the DALI server (22) did not identify structures with significant similarity to the nsp15 monomer or its C-terminal domain. When the N-terminal and central domains together were used as a structural query, no hit was returned at all. Thus, both the overall fold of each domain and the domain organization of nsp15 appear to be undocumented.

nsp15 Is a Hexamer. Examination of the crystal packing of nsp15 suggested a hexameric structure (110 × 80 Å), formed by a dimer of trimers located around the cubic threefold axis. This observation is consistent with previously reported transmission electron microscopy data (17) as well as gel filtration experiments (data not shown) (23). Each trimer is ring-shaped, and the juxtaposition of the two trimers creates a narrow tunnel with a diameter of 15 Å in the center of the hexamer (Fig. 1 *c* and *e*). The three subdomains of the monomer are shown in Fig. 1 (Fig. 1 *c* and *d*). The N-terminal domain mediates most of the critical intermolecular interactions

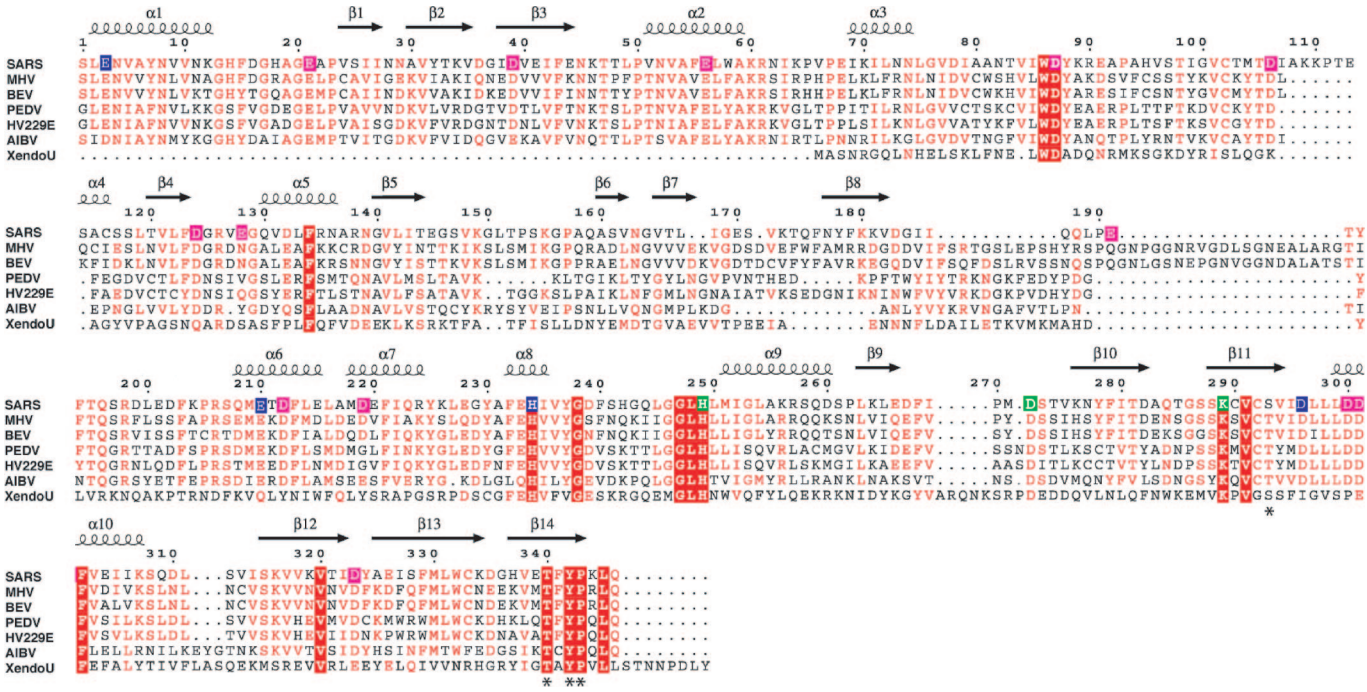

Fig. 2. Sequence alignment of nsp15 from SARS-CoV and other coronaviruses as well as XendoU from *X. laevis*. The numbering refers to the SARS-CoV nsp15 sequence (SARS). nsp15 secondary structures are shown above the sequences. Several mutants of nsp15 have been previously reported (16, 17). Enzymes are shown with substitutions of residues highlighted in the following colors: blue, substitutions were affected in both their enzymatic activity and oligomerization state; pink, substitutions revealed enzymes with wild-type properties; green, substitutions affected the activity but not the oligomerization state. The four amino acids highlighted by an asterisk are the ones mutated in the present study. Fully conserved residues are shown in red. MHV, mouse hepatitis virus strain 2; BCoV, bovine coronavirus (strain 98TXSF-110-ENT); PEDV, porcine epidemic diarrhea virus (strain CV777); HV229E, HCoV-229E; AIBV, avian infectious bronchitis virus (strain Beaudette).

that appear to drive the formation of trimers, including interactions with the central and C-terminal domains of the adjacent monomer (Fig. 1 *c–f*). Moreover, the N-terminal domains are placed at the interface between the trimers (Fig. 1*d*), where they form a platform that supports the formation of the hexamer: as many as 45 (of 51) amino acids of the N-terminal subdomain are involved in trimer–trimer interactions. Conversely, as shown in Fig. 1 *c* and *d*, the C-terminal domain (in red) is far away from the trimer–trimer interface. The C terminus is mostly solvent-exposed and protrudes out of the hexamer core, forming the petals of a flower (Fig. 1 *c–f*). Accordingly, the C-terminal domains are involved in intratrimer interactions and not in the interactions between the two trimers. Approximately 13% (2,200 Å^2) of each monomer's water-accessible surface area is involved in the interactions forming the trimer, half of this surface with each of the other two molecules. Each monomer interacts only with one molecule from the other trimer, with an interaction surface area of 803 Å^2, representing only 4.7% of the monomer's water-accessible surface area.

Mutational Studies. Previously, mutational studies (16, 17) have identified residues that are essential for nsp15 endonuclease activity. Ala substitutions of Asp-272, Lys-289, His-234, or His-249 (Fig. 2) completely abolished nucleolytic activity, whereas Ala substitutions of Glu-3 and Glu-210, respectively, reduced this activity. In human coronavirus 229E (HCoV-229E) nsp15, Ala mutations of Asp-6408 and Asp-6435 (corresponding to Asp-296 and Asp-323 in the SARS-CoV homolog) led to inactivation of nsp15. Asp-272 is located at the interface between the C-terminal and central domains, suggesting an important role for the stability of the nsp15 monomer. Indeed, the nsp15 D272A mutant was reported to be unstable in solution (17). Glu-210 is located in the core of the C-terminal domain, where it is part of an H-bond network between several secondary structures. Glu-3, by contrast, is located on the protein surface. It is involved in trimer–trimer interactions by forming two H-bonds with one of the monomers from the other trimer. Consistent with this observation, Guarino *et al.* (17) reported that a significant proportion (52%) of the nsp15 E3A mutant is monomeric, supporting a critical role of this residue in oligomerization. Taken together, the structural and functional information suggests that the enzymatic defects seen in the D272A, E210A, and E3A mutants are due to indirect effects, most probably structural destabilization of the protein, rather than affecting directly catalysis and/or substrate binding. The results obtained for Asp-296 and Asp-323 substitutions are even less conclusive: D323A abolished the nsp15 activity in HCoV-229E but not in SARS-CoV, and D296A inactivated HCoV-229E nsp15, whereas the corresponding SARS-CoV D296A mutant could not be obtained in a soluble form (17). In our structure, both of these Asp residues lie in the core of the C-terminal domain and are involved in an extensive H-bond network, with Asp-296 forming five hydrogen bonds and Asp-323 forming seven. This H-bond network is close to, but not directly located in, the putative active site. We therefore believe that the latter two Asp substitutions have structural effects on nsp15 that indirectly impair the activity of the protein. In this context, the recent study by Posthuma *et al.* (24) is of particular interest. It was shown that substitutions of the two presumed catalytic His residues in the equine arteritis virus NendoU homolog caused a small-plaque phenotype and dramatic losses in virus titers, but, surprisingly, the His substitutions had only moderate effects on viral RNA synthesis. By contrast, substitutions of the Asp residues equivalent to Asp-296 and Asp-323 in the SARS-CoV nsp15 blocked equine arteritis virus RNA synthesis completely, and no viable virus could be obtained. Taken together, the structural and functional data suggest that the catalytic activity of NendoU has important functions in the nidovirus replication cycle and that the structural integrity of nsp15 is absolutely essential for viral replication.

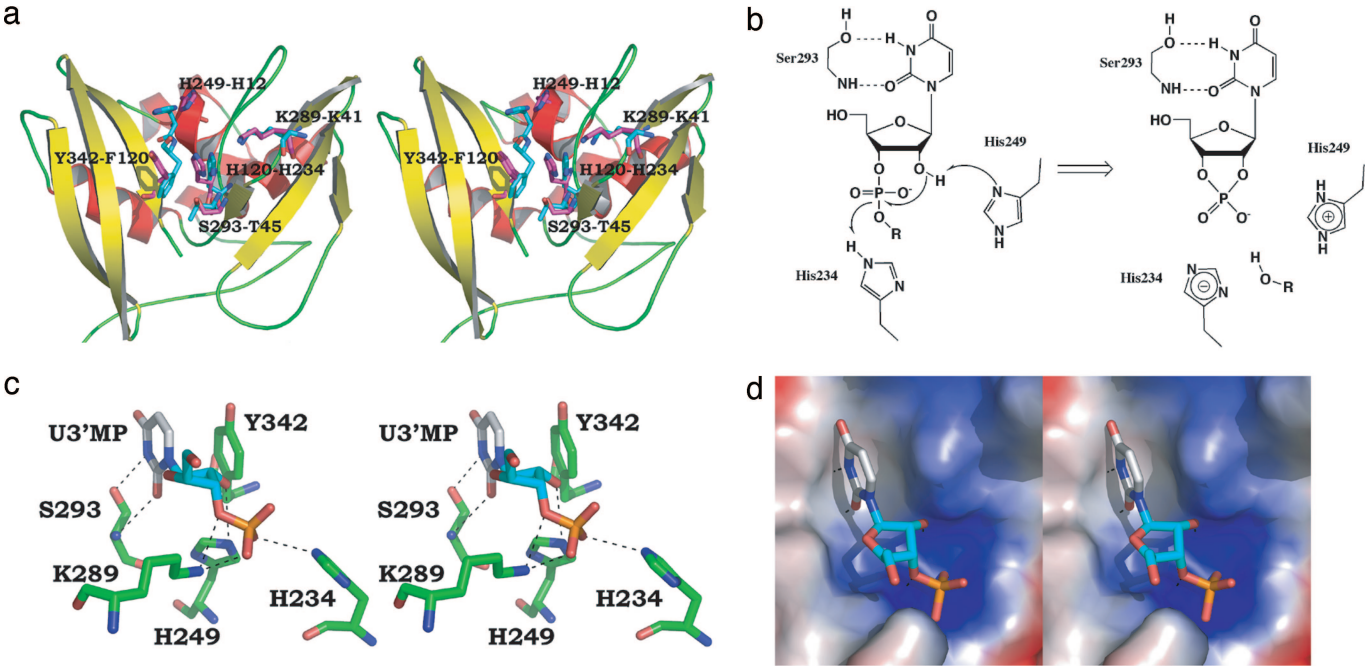

Fig. 3. Catalytic site and proposed enzymatic mechanism. (*a*) Stereoview of the active site groove formed by the nsp15 C-terminal domain. The catalytic amino acids of bovine pancreatic RNase A (in cyan) are superimposed with the putative catalytic amino acids of nsp15 (in magenta). (*b*) Proposed enzymatic mechanism as suggested by the SARS-CoV nsp15 crystal structure and mutational studies, in analogy with the mechanism established for bovine pancreatic RNase A. (*c*) Stereoview of uridine 3′-phosphate (U3′MP) modeled in the nsp15 active site. The main hypothetical interactions between the catalytic amino acids and U3′MP are shown as dashed lines. (*d*) Stereoview of the electrostatic potential of the nsp15 active site groove. The modeled U3′MP molecule is shown in ball and stick representation.

The nsp15 Active Site and Uridyl Specificity. The tunnel traversing the hexamer is too narrow to accommodate an RNA substrate, a feature proposed for the nsp7–nsp8 complex (11). Moreover, Glu-44 side chains protrude into the tunnel, rendering its surface negatively charged, a feature that is not compatible with RNA binding. The active site, therefore, should be located elsewhere. Previous mutational studies have identified Asp-272, Lys-289, His-234, and His-249 as essential residues for nsp15 endonuclease activity (Fig. 2) (16, 17). Based on these data as well as on sequence comparisons of nidovirus and cellular nucleases, a catalytic center involving Lys-289, His-234, and His-249 was proposed (17, 25). In our structure, the three putative catalytic residues, Lys-289, His-234, and His-249, are indeed gathered together in a positively charged groove in the C-terminal domain, far from any monomer–monomer interfaces (Fig. 1 *e* and *f*), implying that the nsp15 hexamer contains six independent active sites.

Interestingly, bovine pancreatic RNase A, for which the catalytic mechanism has been well characterized, also employs two His residues and one Lys residue in its active site (His-12, Lys-41, and His-119). In this case, His-12 and His-119 act as general base and general acid, respectively, whereas Lys-41 interacts with the phosphate moiety to stabilize the pentacovalent intermediate (21). Superimpositions of the nsp15 and RNase A tertiary structures or the loops bearing the three essential His and Lys residues proved to be impossible. In contrast, however, the Lys-289, His-249, and His-234 residues of the SARS-CoV nsp15 could be superimposed very nicely onto the RNase A Lys-41, His-12, and His-119 residues with a rms deviation for C^{α} of 0.3 Å (Fig. 3*a*), indicating that, as reported for other catalytic machineries (e.g., that of nucleic acid polymerases), the relative positions of the key active-site residues are much better conserved than are the general or local protein folds.

Besides the catalytic His–His–Lys triad, two other amino acids, Thr-45 and Phe-120, are known to be important for catalysis in RNase A and its closest relatives. In RNase A, Thr-45 is responsible for the pyrimidine specificity on the 3′ side of the cleavage site (21). In RNase T1, Phe-100 (corresponding to Phe-120 in RNase A) makes stacking interactions with the ribonucleotide base and its phosphate moiety, which likely contributes to the proper positioning of the ribonucleotide in the active site (26). Superimposition of the RNase A catalytic triad with the nsp15 Lys-289, His-234, and His-249 residues revealed that the positions of the nsp15 Ser-293 and Tyr-342 residues corresponded to those of the Thr-45 and Phe-120 residues of RNase A (Fig. 3*a*). Similar to the Phe-120 in RNase A, the aromatic ring of the nsp15 Tyr-342 might establish van der Waals interactions with the uracil moiety in the active site. Alternatively, Tyr-342 could merely narrow the groove, thereby positioning the substrate appropriately for the reaction (Fig. 3 *c* and *d*). To further assess the significance of these residues, we performed several substitutions in nsp15, focusing on a C-terminal conserved amino acid patch (T340A, Y342A, and P343A). As shown in Fig. 6, which is published as supporting information on the PNAS web site, Pro-343 and Tyr-342 proved to be critically involved in activity (see *Discussion*).

Furthermore, the excellent superimposition of the SARS-CoV nsp15 Ser-293 and RNaseA Thr-45 residues (Fig. 3*a*) as well as the known role of Thr-45 in the pyrimidine specificity of RNase A prompted us to investigate the function of Ser-293. We substituted this residue and measured the nsp15 endonuclease activity of the mutant. As predicted, the activity was significantly decreased but not completely abolished (Fig. 6 *A*, lane 5, and *B*, lane 5). The final intermediate cleavage product and some of the intermediate cleavage products corresponded well to those produced by the wild-type enzyme (Fig. 6*A*) (16), arguing against major changes in the specificity of the mutant. Although compatible with a role of Ser-293 in substrate binding, the data suggest that yet other residues must contribute to the pronounced uridylate specificity of the enzyme. In other CoV nsp15s and XendoU, the position of the SARS-CoV nsp15 Ser-293 residue is occupied by a conserved Thr residue (Fig. 2), providing additional support for the hydroxyl

functionality playing a role in a conserved mechanism. This hypothesis receives strong support from mutagenesis data obtained for HCoV-229E nsp15 (16), which showed that the replacement of the conserved Thr residue (Ser-293 in SARS-CoV) resulted in significantly reduced ribonuclease activity. Another residue that could be involved in substrate recognition is the conserved Thr-340. Also in this case, a substitution by Ala caused a significant reduction in activity, but again, no apparent change in specificity was observed. Structure information on a binary complex will be required to elucidate or even manipulate the enzyme's specificity determinants.

Discussion

The unparalleled size of the coronavirus RNA genome and the special mechanisms used by these viruses and their closest nidovirus relatives to produce an extensive set of subgenomic RNAs is linked to a replicative machinery of unusual complexity that also includes a stunning variety of enzymatic activities unique among RNA viruses. The biological functions (or even structures) of these multiple activities are only slowly beginning to emerge (1, 4, 7, 27). Based on its homology with XendoU (18), nsp15 could be identified as a novel RNA virus endonuclease activity (7, 15, 16). The SARS-CoV nsp15 crystal structure that we present here at 2.6-Å resolution reveals a unique fold that leads us to propose a previously undescribed family, endoU, of RNA endonucleases. To date, this family encompasses two distantly related groups of cellular (prototyped by XendoU) and viral (prototyped by the coronavirus nsp15) uridylate-specific endoribonucleases. Although endonucleases are ubiquitous enzymes that are involved in many aspects of RNA metabolism, they are extremely rare in the RNA virus world, with only very few exceptions. Thus, for example, orthomyxoviruses carry in their PB1 replicase subunit an endonuclease activity dedicated to cap-snatching; the pestivirus glycoprotein E^{rns} exhibits an endonuclease activity involved in counteracting the host IFN response; and retrovirus reverse transcriptases employ RNase H activities to remove the RNA template during retroviral DNA synthesis. None of these activities are structurally or enzymatically related to the NendoU of nidoviruses.

In general, viruses have evolved a number of strategies to protect their genomes from host nucleases. In (−)RNA viruses, the viral ssRNA is generally coated with nucleoprotein, protecting the viral RNA from cellular nuclease attack. (+)RNA viruses, on the other hand, counteract cellular responses triggered by dsRNA by inducing and employing specific membrane compartments that protects the viral RNA from cellular nucleases, at least up to the stage where the (+)RNA is being used as a messenger RNA that directs viral protein synthesis. Based on these considerations, it is safe to assume that nidoviruses have evolved a mechanism that regulates and tightly controls the NendoU activity so as to act specifically on as-yet-unknown substrates in a tightly controlled manner. Potential mechanisms involved in the control of the NendoU activity have not been identified, but it has been suggested that they involve the ribose-2′-*O*-methyltransferase (nsp16) activity conserved in corona-, toro- and roniviruses (16). This hypothesis is based mainly on the fact that 2′-*O*-methylated RNA is protected from nsp15-directed cleavage. Both the conservation of a multitude of enzymatic activities in nidoviruses and the specific features of the nidovirus life cycle indicate that nidoviruses have evolved currently unknown pathways to (*i*) regulate the activity of their RNA-dependent RNA polymerase, (*ii*) modulate processes ancillary to replication, or (*iii*) counteract innate immunity-related mechanisms of the host cell. The available evidence suggests that NendoU may be part of (some of) these nidovirus-specific pathways.

Nsp15 is shown here to have an unusual structure made up by six monomers bearing six independent catalytic sites that are assembled into a large complex of toric shape. The interaction surface area between the subunits ranges between 800 and 1,100 $Å^2$, which is within the range of values reported for, e.g., Ig domain protein complexes. This surface area, however, represents only between 4.7% and 6.5% of the whole monomer surface, which already is in the twilight zone for assessing strong quaternary assembly (28). This result may explain why, depending on the technique used, monomers, trimers, and hexamers of nsp15 have been observed (17). Indeed, during crystallization, which requires high protein concentration, the equilibrium may be shifted toward the hexameric form. Surprisingly, the central hole is too narrow to accommodate an RNA molecule, and the six active sites are peripheral. The architecture suggests that nsp15 might be tethered to other partners connecting this hexameric assembly to the replication complex or that nsp15 may affect cellular processes not directly related to viral RNA synthesis.

The low-resolution hexameric structure reported previously for nsp15 (17) indicated that nsp15 might be a hexamer and provided first insights into its shape. It turned out to be impossible to fit our hexamer structure in the previously reported nsp15 contour, whereas the two individual trimers could be fitted readily (Fig. 7, which is published as supporting information on the PNAS web site). Nevertheless, there were significant inconsistencies between our x-ray structure and the EM data. First, the central hole in the EM shape is twice as large as the one in the crystal structure. Secondly, the distance between the fitted trimers in the EM shape is too large for direct contacts to be established. The staining techniques used by the authors of the EM study might have caused deformations. Furthermore, the 2D crystals were oriented in such a way that the trimer–trimer distance could not be estimated. In conclusion, we think that the gross features of the trimer shape, but not the assembly of the hexamer, are reasonably reflected by the EM study.

Although the general fold of nsp15 does not resemble the structures of any other endoribonucleases, striking similarities have been observed between the geometries of the RNase A active site and what we propose to be the nsp15 active site. A uridine 3′-monophosphate molecule modeled in the active site suggests that a reaction similar to that performed by RNase A is conceivable. The catalytic His-234 and His-249 are properly positioned to accept and donate protons, as shown in Fig. 3*b*. The proposed mechanism also is consistent with experimental data obtained for nsp15: DNA or 2′-*O*-methylated RNA cannot be cleaved by nsp15 because, obviously, there is no 2′-OH that could be deprotonated by His-249. Furthermore, the proposed catalytic mechanism leads to a product with a 2′–3′ cyclic phosphate (16). However, in this model of nsp15-mediated catalysis, the role of the Mn^{2+} ions, which are known to be essential for activity, remains unclear. Experimental evidence suggests that Mn^{2+} is not essential for RNA binding to XendoU (25) and that the nsp15 oligomerization state is not dramatically changed by Mn^{2+} ions (17). Tryptophan fluorescence data, however, revealed that Mn^{2+} ions induce conformational changes in the protein (15), pointing to a structural role of these ions, for example to induce a switch to the catalytically active conformation. To date, our structural results do not confirm nor exclude this hypothesis and, clearly, a complex of nsp15 with Mn^{2+} will be required to resolve this issue. Unfortunately, in our hands, nsp15 proved to be unstable in the presence of Mn^{2+} ions. In this context, it is also worth noting that a Tyr residue (Tyr-342), which is absolutely conserved in the endoU family, is located in close proximity to the catalytically essential ribose 2′-OH group (Fig. 3 *c* and *d*). It is therefore tempting to speculate that Tyr-342 might coordinate a Mn^{2+} ion and thereby play a key role in catalysis. Aromatic residues are known to coordinate cations and metal ions, such as Mg^{2+} and Mn^{2+}, through cation-Π interactions (29). Although long known for their structural role, these interactions have recently been revisited regarding their catalytic potential (30). Thus, for example, the endonuclease EndN was shown to employ Tyr and His residues to coordinate a catalytic Zn^{2+} (31). In this mechanism, an aromatic ring holds a metal ion, which closely interacts with a ligand, such as an hydroxyl group, and the latter is

then activated to perform its function as a nucleophile. Our structure suggests that such a configuration is possible and might involve the ribose 2′-OH group and the Tyr-342 and His-249 residues, which are conserved throughout the endoU family (Fig. 3). But clearly, structure analysis of RNA–nsp15 binary complexes is highly desirable to corroborate such a speculative scenario.

Interestingly, although the active sites of RNase A and nsp15 could not be superimposed, the relative spatial positions of the key catalytic amino acids of the enzymes did superimpose well, which might point to yet another case of convergent evolution of catalytic mechanisms. In terms of phylogeny, however, it seems most likely that the ancestor of the present-day nidoviruses acquired its NendoU domain from a cellular homolog (prototyped by XendoU). The conservation of such a specialized enzyme in the nidovirus replicase adds to the sophisticated beauty of these large viral replication machineries and suggests functional links between nidoviral enzymes and cellular metabolic pathways, which remain to be characterized in future studies.

Materials and Methods

Expression and Purification and Crystallization. Selenomethionine-labeled nsp15 was produced according to published protocols (32). The protein was purified and crystallized under the same conditions as the native enzyme, although it proved to be even less stable in solution than the native nsp15 (23). The crystals grew in the same fashion as those of the native protein and reached a comparable size after 1 week. Crystals belong to the same cubic space group as the native protein, $P4_332$, with unit cell parameters $a = b = c = 166.6$ Å, and 75% of the crystal volume is occupied by solvent (Vm = 5.0), with one molecule in the asymmetric unit (33). Attempts to obtain complexes of nsp15 with short RNAs have been unsuccessful, and addition of Mg^{2+} ions caused the protein to precipitate.

Data Collection, Structure Determination, and Refinement. Crystals of selenomethionine-labeled protein were cryoprotected with 33% glycerol, and data were collected at 110 K. nsp15 single-wavelength anomalous dispersion data collection was carried out on the tunable beamline ID23 at the European Synchrotron Radiation Facility equipped with a MAR Marmosaic 225 charged-coupled device detector. Data were processed with MOFLM/SCALA (34, 35). Because the intensity of the diffraction was rather weak, we aimed to collect a high redundant data set to improve the quality of processed data. Phases were calculated at 4.0 Å with the program SHELXD (36), which located all six selenium sites. Subsequently, phase refinement, density modifications, and phase extension to 2.9 Å were performed with RESOLVE (37), yielding a partial model with which ≈40% of the main chain was traced. Manual model building was then carried out with COOT (38). Refinement of the model was done with REFMAC5 (39), using the maximum likelihood residual, anisotropic scaling, and bulk refinement correction; hydrogen atoms were generated during cycles of refinement. The model was refined with native data extending up to 2.6 Å.

The analysis of the monomer and trimer interfaces was done with the protein–protein interaction server (www.biochem.ucl.ac.uk/bsm/PP/server), and the analysis of the enzyme geometry was performed with COOT and PROCHECK (38, 40). The topology of nsp15 was analyzed by using the protein topology homepage (www3.ebi.ac.uk/tops). The structures of nsp15 and RNase A were superimposed by using molecule superposition in CCP4 (34). Pictures and electrostatic potential surfaces were generated with PyMol (DeLano Scientific, South San Francisco, CA), and the topology diagram was produced with Topdraw (41).

We thank Claire Debarnot, Nicolas Brémond, Sacha Grisel, Karen Dalle, and Violaine Lantez for help with protein production and crystallization. This work was supported in part by Marseille-Nice Genopole, by Grant QLG2-CT-2002-00988 from the European Union Structural Proteomics in Europe Fifth Programme Cadre de Recherche et Développement Technologique, and by Euro–Asian SARS–DTV Network Grant SP22-CT-2004-511064. The work of J.Z. and R.U. was supported by the Euro–Asian SARS-DTV network and by Deutsche Forschungsgemeinschaft Grant SFB479.

1. Gorbalenya, A. E., Enjuanes, L., Ziebuhr, J. & Snijder, E. J. (2006) *Virus Res.* **117,** 17–37.
2. Siddell, S., Ziebuhr, J. & Snijder, E. J. (2005) in *Topley and Wilson's Microbiology and Microbial Infections*, eds. Mahy, B. W. J. & ter Meulen, V. (Hodder Arnold, London), Vol. 1, pp. 823–856.
3. Brierley, I., Digard, P. & Inglis, S. C. (1989) *Cell* **57,** 537–547.
4. Ziebuhr, J., Snijder, E. J. & Gorbalenya, A. E. (2000) *J. Gen. Virol.* **81,** 853–879.
5. Peiris, J. S., Yuen, K. Y., Osterhaus, A. D. & Stohr, K. (2003) *N. Engl. J. Med.* **349,** 2431–2441.
6. Rota, P. A., Oberste, M. S., Monroe, S. S., Nix, W. A., Campagnoli, R., Icenogle, J. P., Penaranda, S., Bankamp, B., Maher, K., Chen, M. H., *et al*. (2003) *Science* **300,** 1394–1399.
7. Snijder, E. J., Bredenbeek, P. J., Dobbe, J. C., Thiel, V., Ziebuhr, J., Poon, L. L., Guan, Y., Rozanov, M., Spaan, W. J. & Gorbalenya, A. E. (2003) *J. Mol. Biol.* **331,** 991–1004.
8. Yang, H., Yang, M., Ding, Y., Liu, Y., Lou, Z., Zhou, Z., Sun, L., Mo, L., Ye, S., Pang, H., *et al*. (2003) *Proc. Natl. Acad. Sci. USA* **100,** 13190–13195.
9. Sutton, G., Fry, E., Carter, L., Sainsbury, S., Walter, T., Nettleship, J., Berrow, N., Owens, R., Gilbert, R., Davidson, A., *et al*. (2004) *Structure (London)* **12,** 341–353.
10. Egloff, M. P., Ferron, F., Campanacci, V., Longhi, S., Rancurel, C., Dutartre, H., Snijder, E. J., Gorbalenya, A. E., Cambillau, C. & Canard, B. (2004) *Proc. Natl. Acad. Sci. USA* **101,** 3792–3796.
11. Zhai, Y., Sun, F., Li, X., Pang, H., Xu, X., Bartlam, M. & Rao, Z. (2005) *Nat. Struct. Mol Biol.* **12,** 980–986.
12. Saikatendu, K. S., Joseph, J. S., Subramanian, V., Clayton, T., Griffith, M., Moy, K., Velasquez, J., Neuman, B. W., Buchmeier, M. J., Stevens, R. C. & Kuhn, P. (2005) *Structure (London)* **13,** 1665–1675.
13. Ivanov, K. A., Thiel, V., Dobbe, J. C., van der Meer, Y., Snijder, E. J. & Ziebuhr, J. (2004) *J. Virol.* **78,** 5619–5632.
14. Minskaia, E., Hertzig, T., Gorbalenya, A. E., Campanacci, V., Cambillau, C., Canard, B. & Ziebuhr, J. (2006) *Proc. Natl. Acad. Sci. USA* **103,** 5108–5113.
15. Bhardwaj, K., Guarino, L. & Kao, C. C. (2004) *J. Virol.* **78,** 12218–12224.
16. Ivanov, K. A., Hertzig, T., Rozanov, M., Bayer, S., Thiel, V., Gorbalenya, A. E. & Ziebuhr, J. (2004) *Proc. Natl. Acad. Sci. USA* **101,** 12694–12699.
17. Guarino, L. A., Bhardwaj, K., Dong, W., Sun, J., Holzenburg, A. & Kao, C. (2005) *J. Mol. Biol.* **353,** 1106–1117.
18. Laneve, P., Altieri, F., Fiori, M. E., Scaloni, A., Bozzoni, I. & Caffarelli, E. (2003) *J. Biol. Chem.* **278,** 13026–13032.
19. Nowotny, M., Gaidamakov, S. A., Crouch, R. J. & Yang, W. (2005) *Cell* **121,** 1005–1016.
20. Cuchillo, C. M., Pares, X., Guasch, A., Barman, T., Travers, F. & Nogues, M. V. (1993) *FEBS Lett.* **333,** 207–210.
21. Fersht, A. (2000) *Structure and Mechanism in Protein Science* (Freeman, New York).
22. Holm, L. & Sander, C. (1995) *Trends Biochem. Sci.* **20,** 478–480.
23. Ricagno, S., Coutard, B., Grisel, S., Bremond, N., Dalle, K., Tocque, F., Campanacci, V., Lichiere, J., Lantez, V., Debarnot, C., *et al*. (2006) *Acta Crystallogr. F* **62,** 409–411.
24. Posthuma, C. C., Nedialkova, D. D., Zevenhoven-Dobbe, J. C., Blokhuis, J. H., Gorbalenya, A. E. & Snijder, E. J. (2006) *J. Virol.* **80,** 1653–1661.
25. Gioia, U., Laneve, P., Dlakic, M., Arceci, M., Bozzoni, I. & Caffarelli, E. (2005) *J. Biol. Chem.* **280,** 18996–19002.
26. Doumen, J., Gonciarz, M., Zegers, I., Loris, R., Wyns, L. & Steyaert, J. (1996) *Protein Sci.* **5,** 1523–1530.
27. Ziebuhr, J. (2004) *Curr. Opin. Microbiol.* **7,** 412–419.
28. Janin, J. & Rodier, F. (1995) *Proteins* **23,** 580–587.
29. Dougherty, D. A. (1996) *Science* **271,** 163–168.
30. Zaric, S. D., Popovic, D. M. & Knapp, E. W. (2000) *Chemistry* **6,** 3935–3942.
31. Volbeda, A., Lahm, A., Sakiyama, F. & Suck, D. (1991) *EMBO J.* **10,** 1607–1618.
32. Doublie, S. (1997) *Methods Enzymol.* **276,** 523–530.
33. Matthews, B. W. (1968) *J. Mol. Biol.* **33,** 491–497.
34. Leslie, A. G. W. (1992) *Joint CCP4 and ESF-EACMB Newsletter on Protein. Crystallography* (Daresbury Lab., Warrington, U.K.), Vol. 26.
35. Collaborative Computational Project (1994) *Acta Crystallogr. D* **50,** 760–763.
36. Schneider, T. R. & Sheldrick, G. M. (2002) *Acta Crystallogr. D* **58,** 1772–1779.
37. Terwilliger, T. C. & Berendzen, J. (1999) *Acta Crystallogr. D* **55,** 849–861.
38. Emsley, P. & Cowtan, K. (2004) *Acta Crystallogr. D* **60,** 2126–2132.
39. Murshudov, G. N., Vagin, A. A. & Dodson, E. J. (1997) *Acta Crystallogr. D* **53,** 240–255.
40. Laskowski, R. A., Moss, D. S. & Thornton, J. M. (1993) *J. Mol. Biol.* **231,** 1049–1067.
41. Bond, C. S. (2003) *Bioinformatics* **19,** 311–312.